

# CHEMISTRY

## A European Journal

A Journal of



### Accepted Article

**Title:** A Structural and Functional Model for the Tris-Histidine Motif in Cysteine Dioxygenase

**Authors:** Karunanithi Anandbabu, Ramamoorthy Ramasubramanian, Hubert Wadepohl, Peter Comba, Neethinathan Johnee Britto, Madhavan Jaccob, and Ramasamy Mayilmurugan

This manuscript has been accepted after peer review and appears as an Accepted Article online prior to editing, proofing, and formal publication of the final Version of Record (VoR). This work is currently citable by using the Digital Object Identifier (DOI) given below. The VoR will be published online in Early View as soon as possible and may be different to this Accepted Article as a result of editing. Readers should obtain the VoR from the journal website shown below when it is published to ensure accuracy of information. The authors are responsible for the content of this Accepted Article.

**To be cited as:** *Chem. Eur. J.* 10.1002/chem.201901005

**Link to VoR:** <http://dx.doi.org/10.1002/chem.201901005>

Supported by  
**ACES**

WILEY-VCH

# A Structural and Functional Model for the Tris-Histidine Motif in Cysteine Dioxygenase

Karunanithi Anandababu,<sup>[a]</sup> Ramamoorthy Ramasubramanian,<sup>[a]</sup> Hubert Wadepohl,<sup>[b]</sup> Peter Comba,<sup>[b]</sup> Neethinathan Johnee Britto,<sup>[c]</sup> Madhavan Jaccob,<sup>[c]</sup> and Ramasamy Mayilmurugan<sup>[a]</sup>\*

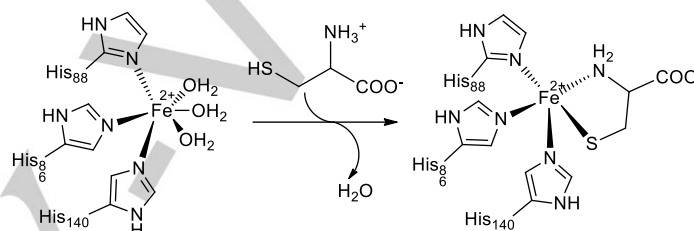
Dedicated to Professor Gabor Laurenczy on occasion of his 65<sup>th</sup> birthday

**Abstract:** The iron(II) complexes [Fe(L)(MeCN)<sub>3</sub>](SO<sub>3</sub>CF<sub>3</sub>)<sub>2</sub> (L are two derivatives of tris(2-pyridyl)-based ligands) have been synthesized as models for cysteine dioxygenase (CDO). The molecular structure of one of the complexes exhibits octahedral coordination geometry and the Fe-N<sub>py</sub> bond lengths [1.953(4) - 1.972(4) Å] are similar to those in the Cys-bound Fe<sup>II</sup>-CDO; Fe-N<sub>His</sub>: 1.893 - 2.199 Å. The iron(II) centers of the model complexes exhibit relatively high Fe<sup>III/II</sup> redox potentials ( $E_{1/2} = 0.988 - 1.380$  V vs. Fc/Fc<sup>+</sup>), within the range for O<sub>2</sub> activation and typical for the corresponding nonheme iron enzymes. The reaction of *in situ* generated [Fe(L)(MeCN)(SPh)]<sup>+</sup> with excess O<sub>2</sub> in acetonitrile (MeCN) yields selectively the doubly oxygenated phenylsulfenic acid product. Isotopic labeling studies using <sup>18</sup>O<sub>2</sub> confirm the incorporation of both oxygen atoms of O<sub>2</sub> into the product. Kinetic and preliminary DFT studies reveal the involvement of an Fe<sup>III</sup> peroxido intermediate with a rhombic S = ½ Fe<sup>III</sup> center (687-696 nm;  $g \approx 2.46 - 2.48, 2.13 - 2.15, 1.92 - 1.94$ ), similar to the spectroscopic signature of the *low-spin* Cys-bound Fe<sup>III</sup>CDO (650 nm,  $g \approx 2.47, 2.29, 1.90$ ). The proposed Fe<sup>III</sup> peroxido intermediates have been trapped, and the O-O stretching frequencies are in the expected range (approx. 920 and 820 cm<sup>-1</sup> for the alkyl- and hydroperoxido species, respectively). The model complexes have a structure similar to that of the enzyme and structural aspects as well as the reactivity are discussed.

## Introduction

Oxygen activating enzymes are involved in several important biochemical reactions, ranging from drug metabolism and biosynthesis of hormones to detoxification processes.<sup>[1]</sup> Cysteine dioxygenase (CDO) converts selectively L-cysteine (Cys) to L-cysteine sulfinic acid, using O<sub>2</sub> in a key step of the biosynthesis of pyruvate and taurine.<sup>[2]</sup> In mammalian systems, the sulfur metabolism is of significant medicinal interest because higher levels of cysteine have been associated with a variety of neurological disorders, including motor neuron, Alzheimer's and Parkinson's disease.<sup>[3]</sup> CDO has been isolated from mouse, rat and human sources and four crystal structures have been published.<sup>[4]</sup> These reveal that a *high-spin* Fe<sup>II</sup> center is coordinated to three histidine residues (His-86, His-88, His-140), one to three solvent (H<sub>2</sub>O) molecules and a cysteine-tyrosine crosslink (C93-Y157) in the second coordination sphere. The substrate Cys is coordinated to the Fe<sup>II</sup> center in a bidentate mode via RS<sup>-</sup> and RNH<sub>2</sub> donors (Scheme 1).<sup>[4]</sup>

The tris-histidine motif (3-His) in the active site of CDO is different from the typical 2-His-1-carboxylate facial triad adopted in the active site of many non-heme Fe<sup>II</sup> dioxygenases and, in addition to CDO, it is found in the  $\beta$ -diketone dioxygenase (Dke1), gentisate dioxygenase, salicylate dioxygenase, and other oxygenases.<sup>[5]</sup>



**Scheme 1.** Chemical structures of the CDO active site and the CDO-Cys adduct.

The biomimetic chemistry of the 2-His-1-carboxylate motif in Fe<sup>II</sup>-dependent oxygenases has been studied extensively<sup>[5,6]</sup> but there is less knowledge about the properties of tris-His residues, and only a few model systems have been reported so far:<sup>[7-9]</sup> Goldberg and co-workers reported the Fe<sup>II</sup>-thiolate complexes [(<sup>i</sup>Pr<sup>BIP</sup>)Fe<sup>II</sup>(SPh)X] (X = Cl, SO<sub>3</sub>CF<sub>3</sub>) of the bis(imino)pyridine BIP with three nitrogen donors, and their reaction with O<sub>2</sub>, leading to S-oxygenation of the coordinated thiolate ligand.<sup>[7]</sup> The enzyme-substrate model complexes [Fe<sup>II</sup>(N<sub>3</sub>S)(SO<sub>3</sub>CF<sub>3</sub>)] (N<sub>3</sub> = BIP) and [Fe<sup>II</sup>(N<sub>3</sub>PyS)(CH<sub>3</sub>CN)]BF<sub>4</sub> (N<sub>3</sub>Py = N-[di(2-pyridinyl)-methyl]-N-(2-pyridinylmethyl)amine), where the thiolate substrate is linked to the ligand, have also been reported. Oxygenation of these complexes yield selectively the triply S-oxygenated sulfonato product.<sup>[8]</sup> Limberg and co-workers reported cysteine and cystamine adducts of the well-known tris-pyrazolylborate ligand (Tp), serving as biomimetic models of the 3-His-Fe<sup>II</sup> system, and these produce doubly oxygenated products with O<sub>2</sub>.<sup>[9]</sup> Brunold and Fiedler studied Fe<sup>II</sup> complexes of the tris(4,5-diphenyl-1-methyl-imidazol-2-yl)phosphine ligand Ph<sub>2</sub>TIP as a model for the 3-His triad of the thiol dioxygenase (TDO).<sup>[10]</sup>

We use a tris(pyridyl) based ligand system (Scheme 2), which enforces an environment to the metal center (geometry and electronics) that is very similar to the tris-His active site of CDO (vide infra for the observed structural properties; pK<sub>a</sub> (protonated heterocycles): 7.0 vs. 5.2 vs. 2.5 for imidazole, pyridine and pyrazole, respectively). Here, we present results that show that the Fe<sup>II</sup> complex of our ligand is not only a structural model but, upon coordination of a thiolate substrate and reaction with O<sub>2</sub>, produces a *low-spin*

[a] Bioinorganic Chemistry Laboratory/Physical Chemistry, School of Chemistry, Madurai Kamaraj University, Madurai 625021, India. E-mail: [mayilmurugan\\_chem@mkuniversity.org](mailto:mayilmurugan_chem@mkuniversity.org); [ramamayil@gmail.com](mailto:ramamayil@gmail.com)

[b] Universität Heidelberg, Anorganisch-Chemisches Institut und Interdisciplinary Center for Scientific Computing, Im Neuenheimer Feld 270, D-69120 Heidelberg, Germany. E-mail: [peter.comba@aci.uni-heidelberg.de](mailto:peter.comba@aci.uni-heidelberg.de)

[c] Department of Chemistry, Loyola College, Chennai 600034, India. Supporting information for this article is given via a link at the end of the document.

\*These authors contributed equally to this work.

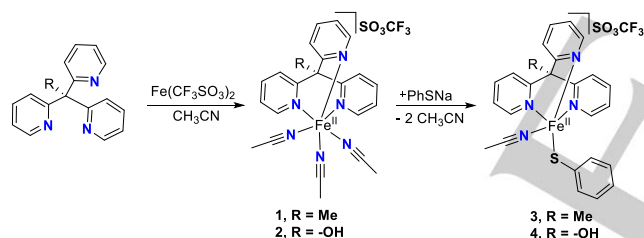
## FULL PAPER

Fe<sup>III</sup>-peroxido intermediate and a doubly oxygenated sulfonic acid as a product.

## Results and Discussion

## Syntheses and Characterization.

The ligands tris(2-pyridyl)ethane and tris(2-pyridyl)-carbinol (L1 and L2, respectively, see Scheme 2) were prepared with a procedure slightly modified to that published before,<sup>[11]</sup> and their Fe<sup>II</sup> complexes were obtained by reaction with Fe(SO<sub>3</sub>CF<sub>3</sub>)<sub>2</sub> in MeCN under argon. Complexes [Fe(L1)(MeCN)<sub>3</sub>](SO<sub>3</sub>CF<sub>3</sub>)<sub>2</sub> **1** and [Fe(L2)(MeCN)<sub>3</sub>](SO<sub>3</sub>CF<sub>3</sub>)<sub>2</sub> **2** were obtained as red-orange solids in good yields (74-82 %). Recrystallization of **1** and **2** in CH<sub>3</sub>CN yielded pure complexes for further studies. The elemental and mass spectrometric analyses (MS) confirm their formation: the HR-ESI-MS shows prominent molecular ion peaks for **1**: [FeN<sub>3</sub>O<sub>3</sub>SC<sub>18</sub>H<sub>15</sub>F<sub>3</sub>]<sup>+</sup> *m/z*, 466.01309 and **2**: [FeN<sub>3</sub>O<sub>4</sub>SC<sub>17</sub>H<sub>13</sub>F<sub>3</sub>]<sup>+</sup> *m/z*, 467.99263 (Figure S1; coordinated solvents may dissociate during the measurement). Attempts to synthesize **1** and **2** with non-coordinating solvents such as CH<sub>2</sub>Cl<sub>2</sub> and CHCl<sub>3</sub> yielded bis-complexes of the type [(L)<sub>2</sub>Fe](SO<sub>3</sub>CF<sub>3</sub>)<sub>2</sub>. This is not surprising since the formation of bis-complexes by structurally similar ligands has been reported for Cu<sup>II</sup>, Fe<sup>II</sup>, Ru<sup>II</sup>, Co<sup>II</sup>, Ni<sup>II</sup>, Zn<sup>II</sup> and Mn<sup>II</sup> complexes,<sup>[12]</sup> and the formation of bis-complexes was only avoided in a few cases by the substitution at the ortho-position of the pyridyl arms of the ligand.<sup>[13]</sup> The solution magnetic susceptibilities of **1** and **2** (Evans method) are  $\mu_{\text{eff}} = 5.1 - 5.3 \mu_{\text{B}}$ , *i.e.* close to the spin-only value for a *high-spin* Fe<sup>II</sup> center. That is, in solution the Fe<sup>II</sup> centers have *high-spin* electronic configuration as in the enzyme.



Scheme 2. Synthesis of the Fe<sup>II</sup> complexes and their adducts.

## Structure, Spectroscopic and Redox Properties.

The unit cell of **2** shows two crystallographically independent molecules with identical coordination geometry and almost identical structural parameters (Supporting Information, Tables S1, S2). In analogy to the three histidine residues (His-86, His-88, His-140) and three water molecules in the active site of CDO, the tris-pyridine ligand and three MeCN molecules complete the octahedral geometry around the Fe<sup>II</sup> center.<sup>[4]</sup> Interestingly, the Fe-N<sub>1py</sub> bond (1.953 (4), 1.958 (4) Å) is slightly shorter than the other two Fe-N<sub>py</sub> bonds (1.969 (4), 1.972 (4) Å, 1.965 (4), 1.965 (4) Å, respectively). A similar but more pronounced difference of the Fe-N<sub>His</sub> bond distances was observed in the active site of a Cys-bound Fe<sup>II</sup>-CDO (Fe-N<sub>His86</sub>, 1.893; Fe-N<sub>His88</sub>, 2.199; Fe-N<sub>His140</sub>, 2.110 Å).<sup>[4,14]</sup> Interestingly, the Fe-N<sub>His</sub> distances are almost identical in the resting state CDO structure (2.0 - 2.1 Å).<sup>[4]</sup> The Fe-N<sub>py</sub> distances in **2** are shorter than the Fe-N<sub>His</sub> bonds in CDO, while those of the Fe<sup>II</sup>-Tp complexes and their derivatives (2.11 - 2.28 Å) are longer, and this is due to

electronic effects (e.g., the pK<sub>a</sub> values, see above) and the geometries (5- vs. 6-ring heterocycles).<sup>[7-10]</sup> The similarity of the structurally well-defined Fe<sup>II</sup> model **2** with that of the enzyme is visualized by the overlay plot of **2** with the active site structure of CDO (Figure 1): the main difference between the two geometries is the torsion around the Fe-N<sub>heterocycle</sub> axes, well visualized in Figure 1. We propose that this is due to the rigidity of our model ligands L, where the only flexibility in the tripodal structure is the torsion around the C<sub>alkyl</sub>-C<sub>heterocycle</sub> bond, and the lowest energy conformation obviously is that with the three pyridine rings parallel to the molecular C<sub>3</sub> axis. However, we anticipate only a minor electronic perturbation due to this major structural difference, since  $\pi$ -bonding involving pyridine and imidazole groups coordinated to an iron center is known to be of only minor importance at most.<sup>[15]</sup> It therefore is not obvious how this structural “mismatch” relates to differences in the reactivities.

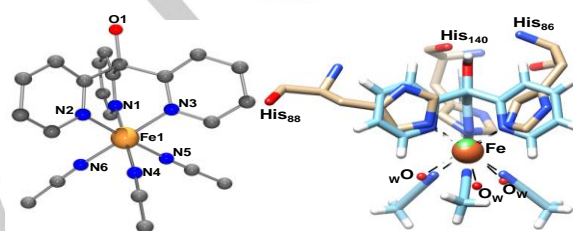


Figure 1. Left: molecular structure of **2**; H-atoms and SO<sub>3</sub>CF<sub>3</sub><sup>-</sup> ions are omitted for clarity. Right: overlay plot of the structures of the CDO active site and **2**.

Due to the inductive effect of the methyl group in L1, the iron complex **1** exhibits a lower Fe<sup>III/II</sup> redox potential ( $E_{1/2}$ , 0.988 V vs. Fc/Fc<sup>+</sup>) than **2** ( $E_{1/2}$ , 1.38 V vs. Fc/Fc<sup>+</sup>, Supporting Information, Figure S2, Table S3). However, the Fe<sup>III/II</sup> potential of **1** is higher than the reported redox barrier for O<sub>2</sub> activation by non-heme iron centers of less than -0.10 V vs. Fc/Fc<sup>+</sup>.<sup>[7,15]</sup> Complex **1** shows electronic absorption bands at 449 nm ( $\epsilon$ , 704 M<sup>-1</sup>cm<sup>-1</sup>) and 383 nm ( $\epsilon$ , 3172 M<sup>-1</sup>cm<sup>-1</sup>), assigned to arise from Fe<sup>II</sup>-to-ligand charge transfer transitions (MLCT),<sup>[16]</sup> and the more intense bands below 342 - 247 nm are due to  $\pi \rightarrow \pi^*$  transitions within the ligand. Very similar transitions are observed for **2**, ( $\lambda$ ,  $\epsilon$ : 438 nm, 1304 M<sup>-1</sup>cm<sup>-1</sup>; 379 nm, 3790 M<sup>-1</sup>cm<sup>-1</sup>; Supporting Information, Figure S3, Table S3). Thiophenol was used as a model substrate for studying CDO-type reactivity in presence of dioxygen. On addition of sodium thiophenolate (PhSNa) to **1** and **2**, there is formation of the thiophenolate adducts [Fe(L1)(MeCN)(SPh)]<sup>+</sup>, **3** (HR-ESI-MS, *m/z*, 467.0955), and [Fe(L2)(MeCN)(SPh)]<sup>+</sup>, **4** (HR-ESI-MS, *m/z*, 469.3512), respectively (Supporting Information, Figure S4). The Fe<sup>III/II</sup> redox potentials of **3** ( $E_{1/2}$ , 1.06 V) and **4** ( $E_{1/2}$ , 1.26 V, Supporting Information, Figure S5, Table S3) are slightly different from those of **1** and **2**. The formation of the thiolate adducts is supported by PhS  $\rightarrow$  Fe<sup>II</sup> charge transfer (CT) transitions around 550 nm (L1) and 560 nm (L2) (Supporting Information, Figure S3, S8). Similar spectral features were observed for the Cys-bound Fe<sup>II</sup>-CDO<sup>[4,6]</sup> as well as in other model complexes.<sup>[7-10]</sup>

All possible electronic spin states of **3** and **4** were optimized using DFT methods. The optimized geometries of **3** and **4** along with computed bond parameters, spin density plots and relative energies between different spin states are given in the Supporting information, Table S4. Calculations reveal that the *high-spin* ( $S = 2$ ) surface is the ground state

## FULL PAPER

for both **3** and **4**. Spin density plots show that the four unpaired electrons are predominantly localized on the metal center ( $\rho_{\text{Fe}} = 3.66$ ). TD-DFT-simulated absorption spectra of *high-spin* **3** show a band at 427 nm, which is due to a charge transfer transition from PhS  $\rightarrow$  Fe<sup>II</sup>. This supports the experimentally observed band at around 550 nm corroborating the formation of thiolate adduct (see Supporting Information, Figure S6).

## Dioxygenation Kinetics and Product Analysis.

On treatment of **3** with O<sub>2</sub> at -40°C, the electronic transition at 550 nm, assigned to a PhS  $\rightarrow$  Fe<sup>II</sup> CT of **3** decreases with a second order reaction rate  $k_{\text{O}_2} = (5.14 \pm 0.09) \times 10^{-2} \text{ M}^{-1} \text{ s}^{-1}$  ( $t_{1/2}$ , 0.46 h; Figure 2, S7, Table S3). Complex **4** shows a decrease in intensity of the PhS  $\rightarrow$  Fe<sup>2+</sup> CT band around 514 nm together with the formation of a transition around 455 nm. The corresponding rate of oxygenation is  $k_{\text{O}_2} = (11.46 \pm 0.01) \times 10^{-2} \text{ M}^{-1} \text{ s}^{-1}$  ( $t_{1/2} = 0.21$  h; Supporting Information, Figure S8, S9; Table 1, S3), *i.e.* two times faster than for **3**. The reaction mixtures from kinetic studies show complete regeneration of **1** and **2**, supported by HR-ESI-MS with prominent ions at  $m/z$ , 466.01312 and  $m/z$ , 467.99215, respectively, for **1** and **2**. The GC-MS analyses of the reaction solutions confirm the formation of the doubly oxygenated phenylsulfonic acid as product. In separate experiments, a 10-fold excess of sodium thiophenolate was treated with the iron complexes **1** and **2** in presence of O<sub>2</sub> at 25°C. After 12 hours, the GC-MS analysis showed 100% conversion of the substrate to phenylsulfonic acid (GC yield: **1**, 98% and **2**, 93%). In contrast to previously reported systems,<sup>[9,10]</sup> no disulfide-bridged dimer product of the substrate or triple oxygenation were observed.

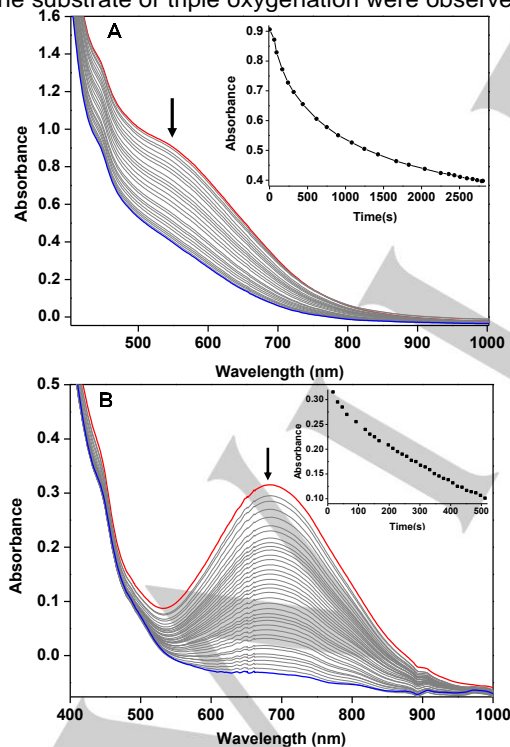


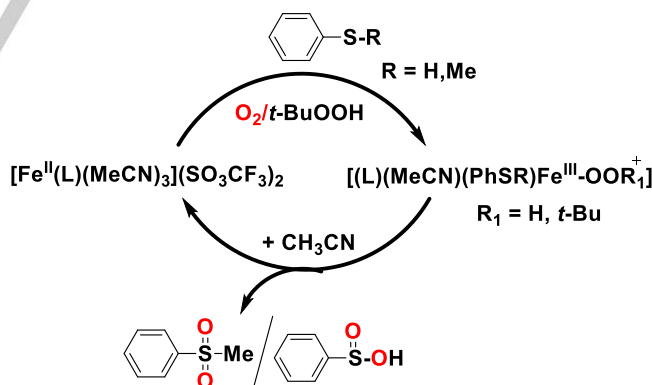
**Figure 2.** (A) UV-vis-NIR spectral changes for the reaction of **3** ( $6 \times 10^{-4}$  M) with saturated O<sub>2</sub> at -40°C and (B) decay of its alkylperoxido-Fe<sup>III</sup> species at 25°C in MeCN. Insets: plot of the change in absorbance vs. time.

Further, the stoichiometric reaction of **1** with thiophenol and thioanisole in presence of O<sub>2</sub> yielded phenylsulfonic acid and methyl phenyl sulfone (GC yield of the latter: 84%), respectively. With <sup>18</sup>O<sub>2</sub> the mass spectra exhibited shifts of four mass units for phenylsulfonic ( $m/z$ , 142 vs. 146) and methyl phenyl sulfone ( $m/z$ , 160 vs. 156; Supporting Information, Figure S10) over 12 h, indicating that both atoms of <sup>18</sup>O<sub>2</sub> are incorporated into the products. However, mixtures of methyl phenyl sulfoxide and methyl phenyl sulfone were observed in the reaction with thioanisole as substrate, when the reaction was stopped after 5 h instead of 12 h reaction time. Mixed labeling experiments using equal amounts of <sup>16</sup>O<sub>2</sub> and <sup>18</sup>O<sub>2</sub> show some selectivity for the pure isotopomers but also some mixed-labeled sulfone product ( $m/z$ , 156 : 158 : 160 = 2.6 : 1 : 1.2 (Supporting Information, Figure S10a).

## Dioxygenation Mechanism.

Adducts **3** and **4** are spectroscopically distinct, allowing to mechanistically interrogate the O<sub>2</sub> activation and study the kinetics of the formation of intermediates. EPR spectra of adducts **3** and **4** in MeOH at ambient atmosphere (Figure 3; Supporting Information, Figure S11, Table 1, S3) reveal signals for at least three different species, a *high-spin* Fe<sup>III</sup> ( $S = 5/2$ ) (**3**:  $g = 8.62, 6.49, 4.30$ ; **4**:  $g = 7.89, 5.61, 4.30$ ), a rhombic *low-spin* Fe<sup>III</sup> ( $S = 1/2$ ) (**3**:  $g = 2.17, 2.07, 2.04$ ; **4**:  $g = 2.47, 2.13, 1.94$ ),<sup>[15,17,18,21]</sup> and minor components at  $g = 12.17$  and  $11.50$  for **3** as well as a signal at  $g = 2.32, 2.09, 1.98$  for **4**, which might correspond to *intermediate-spin* ( $S = 3/2$ ) or *low-spin* ( $S = 1/2$ ) species.<sup>[22]</sup> The *high-spin* Fe<sup>III</sup> signals of **3** and **4** are similar to previously reported *high-spin* Cys-bound Fe<sup>III</sup>-CDO species.<sup>[16,18]</sup>

**Table 1.** EPR parameters, kinetic data and product analysis of **3** and **4**



## FULL PAPER

Complex	EPR parameters <sup>a</sup>	oxygenation studies	
	( <i>g</i> -values)	$\lambda_{\max}$ , nm ( $\epsilon$ , M <sup>-1</sup> cm <sup>-1</sup> )	Kinetic data and product analysis <sup>b</sup>
<b>3</b> + O <sub>2</sub>	9.32, 7.96,	560 (1458)	$k_{\text{obs}} = 4.16 \pm 0.07 \times 10^{-4} \text{ s}^{-1}$ $k_{\text{O}_2} = 5.14 \pm 0.09 \times 10^{-2} \text{ M}^{-1} \text{ s}^{-1}$ $t_{1/2} = 0.46 \text{ h}$ GC Yield = 98%
	5.50, 4.31,	449 (2230)	
	2.48, 2.21,	386 (4265)	
	2.15, 2.06,	339 (5012)	
	1.92	291 (4776)	
	248 (4651)		
<b>3</b> + <i>t</i> -BuOOH	8.19, 5.51,	687 (525)	$k_{\text{obs}} = 9.39 \pm 0.01 \times 10^{-4} \text{ s}^{-1}$ $t_{1/2} = 0.20 \text{ h}$
	4.31, 2.48,	461 (578)	
	2.24, 2.14,	320 (3598)	
	2.05, 1.93	290 (3917)	
		245 (3912)	
<b>4</b> + O <sub>2</sub>	4.36, 2.46,	514 (836)	$k_{\text{obs}} = 9.28 \pm 0.01 \times 10^{-4} \text{ s}^{-1}$ $k_{\text{O}_2} = 11.46 \pm 0.01 \times 10^{-2} \text{ M}^{-1} \text{ s}^{-1}$ $t_{1/2} = 0.21 \text{ h}$ GC Yield = 93%
	2.14, 1.93	378 (3710)	
		342 (4444)	
		292 (4297)	
		248 (4358)	
<b>4</b> + <i>t</i> -BuOOH	8.25, 5.59,	696 (224)	$k_{\text{obs}} = 2.73 \pm 0.01 \times 10^{-3} \text{ s}^{-1}$ $t_{1/2} = 0.07 \text{ h}$
	4.30, 2.46,	441 (1100)	
	2.14, 2.01,	368 (2069)	
	1.93	291 (3375)	
		253 (2845)	

<sup>a</sup>The EPR spectra of complexes and their adducts have been measured in MeOH at 10 K. <sup>b</sup>Sodium thiophenolate (0.013 g, 0.1 mmol) and iron complex (0.01 mmol), MeCN (1 mL) and then exposed to dioxygen and stirred for 30 minutes.  $k_{\text{O}_2} = k_{\text{obs}} / [\text{O}_2]$ , dissolved O<sub>2</sub> concentration in MeCN =  $8.1 \times 10^{-3} \text{ M}$ .<sup>32,33</sup>

Treatment of adduct **4** with O<sub>2</sub> leads to an increase in the intensity of the EPR signals for the *low-spin* Fe<sup>III</sup> species ( $g = 2.46, 2.13, 1.93$ ) with a concomitant decrease of the intensity of the remaining species (Figure 3; Table 1, S3). Adduct **3** shows the clear formation of a *low-spin* Fe<sup>III</sup> ( $S = 1/2$ ) species with less intense EPR signals at  $g = 2.48, 2.15, 1.92$  and a sharp signal for *high-spin* Fe<sup>III</sup> ( $S = 5/2$ ) at  $g = 4.31$ , with smaller signals at  $g = 9.32, 7.96$  and  $5.50$  (Supporting Information, S12, Table S3). The *low-spin* Fe<sup>III</sup> species resemble those of the previously reported  $S = 1/2$  hydroperoxido- and alkylperoxido-Fe<sup>III</sup> intermediates of non-heme iron complexes.<sup>[18-22]</sup> Very similar *low-spin* Fe<sup>III</sup> ( $S = 1/2$ ) rhombic EPR signals ( $g = 2.47, 2.29, 1.90$ ) were reported for the Cys-bound Fe<sup>III</sup>-CDO on treatment with excess azide/CN<sup>-</sup> (Cys-Fe<sup>III</sup>-CDO/azide adduct:  $g = 2.47, 2.29, 1.90$ ; Cys-Fe<sup>III</sup>-CDO/CN<sup>-</sup> adduct:  $g = 2.38, 2.23, 1.93$ ). These are used as chemical models for O<sub>2</sub> to generate *low-spin* Fe<sup>III</sup> ( $S = 1/2$ ) species.<sup>[19]</sup> These observations indicate the involvement of an Fe<sup>III</sup>-peroxido-type intermediate with O<sub>2</sub> (Figure 3; Supporting Information, Figure S12). Remarkably, on treating **1** and **2** with O<sub>2</sub> in the absence of substrate (PhS<sup>-</sup>), no significant spectroscopic changes were observed by UV-vis and EPR spectroscopies and this is interpreted to indicate that, as in the proposed enzymatic mechanism of CDO, O<sub>2</sub> is only activated in the presence of a substrate.<sup>[4]</sup>

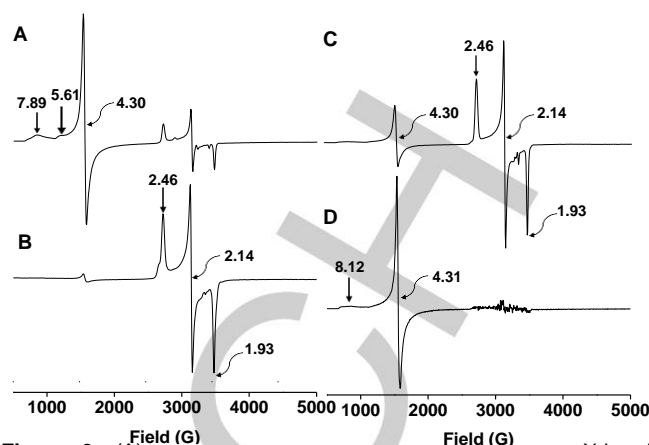


**Figure 3.** (A) X-band EPR spectrum of **4** at ambient atmosphere; (B) with O<sub>2</sub>; (C) on treating with *t*-BuOOH and (D) **2** with *t*-BuOOH in MeOH. EPR parameters: frequency for A, 9.3959; B, 9.3979; C, 9.3966; D, 9.3878 GHz; power = 0.63 mW; modulation amplitude=10 G; modulation frequency = 100 kHz; T = 10 K.

*Tert*-butyl hydroperoxide (*t*-BuOOH) was used as a spectroscopic probe to obtain supplementary mechanistic information. The reaction of freshly generated **3** with *t*-BuOOH at 25 °C in MeCN shows the immediate appearance of an intense green color, assigned to an [(L1)(PhS)Fe<sup>III</sup>-alkylperoxido] species with an LMCT transition at 687 nm (Figure 2; Table 1), and the corresponding EPR signals at  $g = 2.48, 2.14$  and  $1.93$  ( $S = 1/2$  *low-spin* Fe<sup>III</sup> species, Supporting Information, Figure S13, Table 1). Preliminary DFT calculations agree with the experimental observation and their interpretation, where the alkylperoxido-Fe<sup>III</sup> species is found to have a *low-spin* ground-state. The computed relative energies of all possible spin states of the alkylperoxido-Fe<sup>III</sup> species are provided in the Supporting Information, Table S4. The spin density of the single unpaired electron of the *low-spin* Fe<sup>III</sup>-alkylperoxido species is found to be delocalized on the metal center ( $\rho_{\text{Fe}} = 0.76$ ) as well as on the peroxido oxygen atoms ( $\rho_{\text{O}_2} = 0.23$ ). The computed electronic spectrum shows an LMCT band at 681 nm (Supporting Information, Figure S15). The assignment for the alkylperoxido species is confirmed by the HR-ESI-MS analysis (cluster at  $m/z = 727.1396$ , corresponding to [Fe(L1)(MeCN)(SPh)(*t*-BuOO)]SO<sub>3</sub>CF<sub>3</sub>Na<sup>+</sup>, Supporting Information, Figure S16a). The absorption intensity at 687 nm starts to decrease immediately with a rate of  $k_{\text{obs}} = 9.39 \pm 0.01 \times 10^{-4} \text{ s}^{-1}$  ( $t_{1/2}, 0.20 \text{ h}$ ; Supporting Information, Figure S17). A similar green alkylperoxido-Fe<sup>III</sup> species is observed for **4** with an LMCT transition at 696 nm under identical conditions (Supporting Information, Figure S18, S19; Table S3). The *low-spin* Fe<sup>III</sup> EPR signals at  $g = 2.46, 2.14$  and  $1.93$  and a minor signal at  $2.01$  for a *t*-BuOO radical are shown in Figure 3 (see also Table 1). Formation of the alkylperoxido-Fe<sup>III</sup> species is also confirmed by HR-ESI-MS (clusters at  $m/z, 580.1307, 730.0907$ , corresponding to [Fe(L2)(MeCN)(SPh)(*t*-BuOO)]Na<sup>+</sup> and [Fe(L2)(MeCN)(SPh)(*t*-BuOO)]SO<sub>3</sub>CF<sub>3</sub>Na<sup>+</sup>, respectively (Figure S16b). The rate of decay at 696 nm is almost 3 times faster ( $k_{\text{obs}} = 2.73 \times 10^{-3} \text{ s}^{-1}$ ;  $t_{1/2} = 0.07 \text{ h}$ ) than that of **3**. For both model complexes, the GC-MS analysis reveals the formation of phenylsulfonic acid as product.

## FULL PAPER

Further support for the assignment of the observed iron-oxygen intermediates as low-spin hydroperoxido- and alkylperoxido-Fe<sup>III</sup> complexes emerges from solution FT-IR spectroscopy (0°C, MeCN, see Figure 4 and Supporting Information, Figures S21 and S22 as well as the corresponding computational data in the Supporting Information, Table S4). Prominent bands at 923 cm<sup>-1</sup> and 921 cm<sup>-1</sup> upon addition of *t*-BuOOH to the L1- and L2-based Fe<sup>II</sup> complexes **3** and **4** are proposed to originate from O-O vibration of the low-spin iron(III)-bound alkyl peroxide of **3** and **4**. Freshly generated **4** was also treated with H<sub>2</sub>O<sub>2</sub>, and the oxidation product shows a new peak at 824 cm<sup>-1</sup> (see also Figure 4 and Supporting Information, Figure S22), which is proposed to correspond to the O-O vibration of the low-spin hydroperoxido-Fe<sup>III</sup> species. These assignments are supported by published experimental spectra of a range of low-spin (as well as high-spin) hydroperoxido and alkylperoxido iron(III) intermediates (Infra-red and resonance Raman spectroscopy, including <sup>18</sup>O labeling, as well as support by DFT calculations; vibrational frequencies of low-spin Fe<sup>III</sup>-OOH and Fe<sup>III</sup>-OOR species in general are around 790 - 880 cm<sup>-1</sup>, and 800 - 930 cm<sup>-1</sup>, respectively, *i.e.* in the range observed in our experiments).<sup>[5,15,18,23]</sup> Importantly, the O-O vibrational bands of the end-on hydroperoxido and alkylperoxido complexes are supported by the corresponding DFT-computed spectroscopic transitions (see Supporting Information).

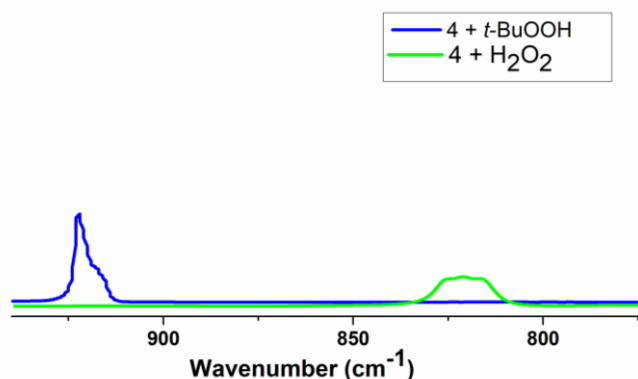


**Figure 4.** Solution FT-IR spectra of the (L2)Fe<sup>III</sup>-hydroperoxido and -alkylperoxido species generated from **4** at 0°C in MeCN by addition of H<sub>2</sub>O<sub>2</sub> or *t*-BuOOH, respectively (see Experimental Section and Supporting Information for details as well as for further spectra and the comparison between experimental and DFT computed spectra).

On treatment of **1** and **2** with *t*-BuOOH, EPR signals for a *high-spin* Fe<sup>III</sup> ( $S = 5/2$ ) species (**1**:  $g = 4.28$ ; **2**:  $g = 8.12$ , 4.31) were detected but no sharp signals for a *low-spin* Fe<sup>III</sup> ( $S = 1/2$ ) species were observed as compared to the corresponding substrate adducts. The entire set of spectroscopic data suggests that the reaction of substrate adducts with O<sub>2</sub> may proceed via the generation of *low-spin* Fe<sup>III</sup>-peroxido intermediates for the oxygenation of the substrate. This is consistent with experimental and TDDFT-derived electronic spectroscopic data, and computed structural parameters of this species are provided in Table S4.

## Summary

An accurate structural model for iron(II)-dependent cysteine dioxygenase enzymes has been synthesized and characterized. The molecular structure of one of the complexes exhibits a very similar coordination geometry as adopted in the CDO enzyme, where Fe-N<sub>py</sub> distances (1.953 - 1.972 Å) are similar to the Fe-N<sub>His</sub> bonds (1.893 - 2.199 Å). The Fe<sup>2+/3+</sup> redox potentials of the complexes and their substrate adducts show higher redox potentials than the reported redox barrier for dioxygen activation. The dioxygenation reaction of the model complex-substrate adducts produces doubly oxygenated products selectively. The kinetics, spectroscopic data and DFT calculations support the involvement of Fe<sup>III</sup>-peroxido species as key intermediates for the dioxygenation reaction. The Fe<sup>III</sup>-peroxido intermediate is characterized as a rhombic  $S = 1/2$  Fe<sup>III</sup> center, similar to the *low-spin* Cys-bound Fe<sup>III</sup> CDO intermediate.

## Experimental Section

**Materials.** The chemicals 2-ethylpyridine, 2-fluoropyridine, di-2-pyridylketone, *n*-butyllithium (2 M in hexane), iron(II) trifluoromethanesulfonate, sodium thiophenolate (PhSNa), (diacetoxyiodo) benzene PhI(OAc)<sub>2</sub>, *tert*-butyl hydroperoxide (*t*-BuOOH), tetrabutylammonium perchlorate (TBAP) and H<sub>2</sub>O<sub>2</sub> were purchased from Sigma-Aldrich. <sup>18</sup>O<sub>2</sub> was purchased from Cambridge Isotope Laboratories. Anhydrous acetonitrile (MeCN), 2-bromo pyridine (Alfa Aesar), tetrahydrofuran (THF) (Merck, India) were used as received. THF was refluxed for an hour over sodium metal and benzophenone and then distilled under N<sub>2</sub> atmosphere, as described in the literature.<sup>[24]</sup> Distilled solvents were degassed and stored under argon over molecular sieves.

**Experimental conditions and physical measurements.** All workup procedures were carried out under dry argon using standard Schlenk line or glove box techniques for the reactions involving air-sensitive experiments. All NMR spectra were recorded on a Bruker 300 MHz spectrometer. Chemical shifts are given in parts per million (ppm). High-Resolution Electron Impact Mass Spectra (HR-ESI-MS) were measured on a Bruker 12 Tesla APEX-Qe FTICR-MS system. UV-vis spectra were recorded on an Agilent 8453 spectrometer with a cooling unit by Unisoku (Osaka, Japan). Elemental analyses were carried out using a Heraeus Vario Elemental automatic analyzer. The EPR experiments were made with a Biospin ELEXSYS E500 spectrometer (Bruker, Karlsruhe, Germany). The EPR spectrometer was equipped with a continuous-flow liquid He cryostat and an ITC503 temperature controller made by Oxford Instruments. Electrochemical data were recorded on a CH Instruments 660 D Electrochemical Workstation. The potentials were externally calibrated against the ferrocene/ferrocenium couple prior to analysis. GC-MS measurements were carried out on Thermo Fischer Scientific Ultra Trace GC / ISQ Single Quadrupole MS and Agilent GC-MS, 7820A GC coupled with 5977E MSD instruments. FT-IR spectra were recorded on a Thermo Nicolet 6700 FT-IR spectrometer.

**Synthesis of tris(2-pyridyl)ethane (L1).** Ligand L1 was synthesized as in an earlier report with modifications.<sup>[25]</sup> The solution of *n*-butyl lithium (14 mL, 28.0 mmol, 2 M in hexane) was added dropwise via a syringe over 15 minutes to 2-ethyl pyridine (1.6 mL, 12.0 mmol, which was pre-cooled to -78°C in THF (40 mL) under argon atmosphere. Then it was stirred vigorously by keeping the temperature below -70°C. After 30 minutes, the solution turns deep red and then 2-fluoropyridine (0.5 mL, 6 mmol) was added dropwise at -20°C. The temperature was slowly brought to room temperature over 30 minutes and then refluxed for additional 30 minutes. Another equivalent of 2-fluoropyridine was then added at 0°C and subsequently refluxed for 2 hours. Finally, the reaction was quenched with water at 0°C and organic materials were extracted with ethylacetate. Volatile compounds were removed in *vacuum*. Pure off-white crystalline solids were obtained by silica column chromatography (7:3 hexane: ethyl

## FULL PAPER

acetate) with a yield of 72% (1.13 g).  $^1\text{H}$  NMR ( $\text{CDCl}_3$ , 300 MHz):  $\delta$ (ppm) 2.33 (s, 3H,  $\text{CH}_3$ ), 7.10 (m, 6H), 7.59 (td, 3H) 8.58 (d, 3H);  $^{13}\text{C}$  NMR ( $\text{CDCl}_3$ , 300 MHz)  $\delta$ (ppm) 27.26 ( $\text{CH}_3$ ), 59.99 (C- $\text{CH}_3$ ), 121.21, 123.43, 135.99, 149.0, 165.72. ESI-Mass,  $m/z$ , 261.05.

**Synthesis of tris(pyridine-2-yl)methanol (L2).** Ligand L2 was also synthesized with slight modifications to an earlier report.<sup>[26]</sup> Then-BuLi (20 mL, 28 mmol, 2.0 M in hexane) was added dropwise to pre-cooled ( $-78^\circ\text{C}$ ) 2-bromopyridine (4.60g, 28mmol) in THF (175 mL) with vigorous stirring and keeping the temperature below  $-70^\circ\text{C}$  under argon atmosphere. This reaction mixture was stirred for 30minutes and then followed by addition of di-2-pyridyl ketone (2.54g, 13.8mmol in THF (25 mL)). It was then stirred for an hour and the deep red solution turned violet. At this point the reaction was quenched by addition of a methanol-water mixture at  $0^\circ\text{C}$  and organic materials were separated with ethylacetate. The removal of ethylacetate under vacuum yielded a pure off-white crystalline solid with a yield of 92% (3.30 g).  $^1\text{H}$  NMR ( $\text{CDCl}_3$ ):  $\delta$ (ppm) 7.19 (td, 3H), 7.71 (m, 6H) 8.58 (dd, 3H);  $^{13}\text{C}$  NMR ( $\text{CDCl}_3$ )  $\delta$ (ppm) 81.21 (C-OH), 122.27,122.90, 136.38, 147.77, 162.80. ESI-MS,  $m/z$ , 263.05.

**Synthesis and characterization of iron(II) complexes.** Iron(II) complexes were synthesized under dry argon using standard Schlenk line and glove box techniques. The ligand (0.5 mmol) was added to iron(II) trifluoromethanesulfonate (0.176 g, 0.5 mmol) in MeCN (10 mL) under argon atmosphere. The reaction mixture was stirred for 2 hours. Then, it was washed with diethylether after removal of the solvent under vacuum to obtain red-orange colored solids.

$[\text{Fe}(\text{L}1)(\text{CH}_3\text{CN})_3](\text{SO}_3\text{CF}_3)_2$ , **1**: Yield, 0.30 g, 82%, HR-ESI Mass,  $m/z$ , 466.01309 corresponds to the  $[\text{FeC}_{18}\text{H}_{15}\text{F}_3\text{N}_3\text{O}_3\text{S}]^+$  ion.

$[\text{Fe}(\text{L}2)(\text{CH}_3\text{CN})_3](\text{SO}_3\text{CF}_3)_2$ , **2**: Yield, 0.27 g, 74%, HR-ESI Mass,  $m/z$ , 467.99263 corresponds to the  $[\text{C}_{17}\text{H}_{13}\text{F}_3\text{FeN}_3\text{O}_4\text{S}]^+$  ion. The crystals from **2** were suitable for single crystal X-ray data structural determination.

$[\text{Fe}(\text{L}1)(\text{CH}_3\text{CN})_3](\text{SO}_3\text{CF}_3)_2$ , **1**: calculated for  $\text{C}_{25}\text{H}_{24}\text{F}_6\text{FeN}_6\text{O}_6\text{S}_2$ : C, 40.66; H, 3.28; N, 11.38%. Found: C, 40.28; H, 3.62; N, 11.47%.  $[\text{Fe}(\text{L}2)(\text{CH}_3\text{CN})_3](\text{SO}_3\text{CF}_3)_2$ , **2**: calculated for  $\text{C}_{24}\text{H}_{22}\text{F}_6\text{FeN}_6\text{O}_7\text{S}_2$ : C, 38.93; H, 3.0; N, 7.54%. Found: C, 38.68; H, 3.20; N, 7.14%.

**X-ray crystallography.** Single crystal X-ray data collection and structure solution. Crystal data and details of the structure determinations are compiled in Table S1, selected bond lengths and angles in Table S2. A full shell of intensity data was collected at low temperature with an Agilent Technologies Supernova-E CCD diffractometer (Mo- $K_\alpha$  radiation, microfocus X-ray tube, multilayer mirror optics). Detector frames (typically  $\omega$ -, occasionally  $\varphi$ -scans, scan width  $0.5^\circ$ ) were integrated by profile fitting.<sup>[27]</sup> Data were corrected for air and detector absorption, Lorentz and polarization effects<sup>[27b]</sup> and scaled essentially by application of appropriate spherical harmonic functions.<sup>[27b,28]</sup> Absorption by the crystal was treated numerically (Gaussian grid).<sup>[28b,c]</sup> An illumination correction was performed as part of the numerical absorption correction.<sup>[28b]</sup> The structures were solved by the charge flip procedure<sup>[29]</sup> and refined by full-matrix least squares methods based on  $F^2$  against all unique reflections.<sup>[30]</sup> All non-hydrogen atoms were given anisotropic displacement parameters. Hydrogen atoms were generally input at calculated positions and refined with a riding model. The positions of the hydroxyl hydrogen atoms were taken from difference Fourier syntheses and refined.

CCDC 1533437 contains the supplementary crystallographic data for this paper. These data can be obtained free of charge from The Cambridge Crystallographic Data Centre via [https://www.ccdc.cam.ac.uk/data\\_request/cif](https://www.ccdc.cam.ac.uk/data_request/cif).

**Evan's method measurements.** The effective magnetic moment was determined by using Evan's method.<sup>[31]</sup> In a typical experiment, an oxygen-free solution of a complexes in  $d_6$ -DMSO, containing 5% *tert*-butanol by volume was placed in an NMR tube, while a reference solution of 5% *tert*-

butanol (v/v) in  $d_6$ -DMSO, was placed into NMR tube insert. Then  $^1\text{H}$ NMR experiments were performed on the Bruker 300 MHz spectrometer and magnetic moment values were obtained by fitting the chemical shift values in the standard equation of the Evan's method.<sup>[31]</sup>

**Kinetics and product analyses.** All iron(II) complexes and substrate solutions were prepared in the glove box. The kinetic analyses of the dioxygenase reactions were carried out by time-dependent measurements of the disappearance of the thiophenolate-to-iron(II) CT band at ambient temperature or at  $-40^\circ\text{C}$  by exposing the thiophenolate adducts (generated *in situ*) to molecular oxygen. Adducts were generated *in situ* by treating the complexes **1** and **2** ( $6.0 \times 10^{-4}$  M) with an equivalent amount of sodium thiophenolate (PhSNa) in MeCN. The solubility of  $\text{O}_2$  in MeCN at  $25^\circ\text{C}$  is  $8.1 \times 10^{-3}$  M.<sup>[32-34]</sup>

In a general method, sodium thiophenolate (0.013 g, 0.1 mmol) and iron complex (0.01 mmol) were added in MeCN (1 mL) and then exposed to dioxygen and stirred over 12 hours. An aliquot of the reaction mixture was filtered through silica gel and analyzed and quantified by GC-MS and  $^1\text{H}$ -NMR spectra. The product was quantified using an authentic sample (purchased from Sigma-Aldrich). Conversions were determined by GC-MS/GC analysis, on an Agilent 7890 Gas Chromatograph-Mass spectrometer. The following temperature program was used: start at  $60^\circ\text{C}$  and keep for 1 min, mount to  $300^\circ\text{C}$  at  $35^\circ\text{C}/\text{min}$ , keep for 1 min and raise to  $320^\circ\text{C}$  at  $20^\circ\text{C}/\text{min}$ .

**Characterization of phenylsulfonic acid (PhSO<sub>2</sub>H).**  $^1\text{H}$ -NMR ( $\text{D}_2\text{O}$ ),  $\delta$ (ppm) 7.79- 7.76 (s, 1H), 7.55-7.52 (s, 1H). IR: 3389, 3053, 1681, 1471, 1069, 968  $\text{cm}^{-1}$ . GC-MS,  $m/z$ , 142.1.

**$^{18}\text{O}_2$  labeling studies.** The mixing of thioanisole (0.0012 g, 0.01 mmol) and complex **1** (0.0061 g, 0.01 mmol) generated an adduct in MeCN (1 mL), and this was exposed to  $^{18}\text{O}_2$  for 12 hours and stirred. An aliquot of the reaction mixture was filtered through silica gel and analyzed and quantified by GC-MS. Mixed labelling experiments were performed under identical condition using a mixture of gaseous  $^{16}\text{O}_2$  and  $^{18}\text{O}_2$ , and stirred for 12 hours. Finally, the reaction mixture was analyzed by GC-MS after similar workup to that described above.

**Computational details.** All the quantum chemical calculations were carried out using Gaussian 09 program.<sup>[35]</sup> For geometry optimization, unrestricted B3LYP functional<sup>[36,37]</sup> with Lan12dz basis set on Fe and 6-31G(d) basis set on rest of the atoms were used. The choice of using B3LYP functional is based on earlier theoretical reports where they show ability in predicting accurate geometrical parameters and provide reliable spin states energetics.<sup>[38,39]</sup> Further the frequency calculation and electronic spectral parameters of sodium thiophenolate adduct and (L1)(PhS)Fe<sup>III</sup>-alkylperoxido species were computed at the same level as that of geometry optimization. For computing the electronic spectrum of species under study, time-dependent density functional theory (TDDFT) method<sup>[40]</sup> was used. In order to improve the energetics, single point energy calculations in MeCN solution were employed using the TZVP basis set on the gas phase optimized geometries. Solvation energies are computed using SCRFP-PCM model.<sup>[41,42]</sup> All the reported spin-state energies are zero-point energy corrected.

## Acknowledgements

We acknowledge SERB, BRNS (India) and DFG (Germany) for funding.

**Keywords:** non-heme iron complexes, dioxygen activation, cysteine dioxygenase, Fe<sup>III</sup> peroxido intermediate, selective dioxygenation.

## FULL PAPER

## References

- [1] M. Sono, M. P. Roach, E. D. Coulter and J. H. Dawson, *Chem. Rev.*, 1996, **96**, 2841; J. T. Groves, *Proc. Natl. Acad. Sci.*, 2003, **100**, 3569; A. W. Munro, H. M. Girvan and K. J. McLean, *Nat. Prod. Rep.*, 2007, **24**, 585.
- [2] J. E. Dominy Jr., L. L. Hirschberger, R. M. Coloso and M. H. Stipanuk, *Biochem. J.*, 2006, **394**, 267; J.-I. Lee, M. Londono, L. L. Hirschberger and M. H. Stipanuk, *J. Nutr. Biochem.*, 2004, **15**, 112; J. E. Dominy Jr., C. R. Simmons, P. A. Karplus, A. M. Gehring and M. H. Stipanuk, *J. Bacteriol.*, 2006, **188**, 5561.
- [3] R. Pean, R. B. Parsons, R. H. Waring, A. C. Williams and D. B. Ramsden, *J. Neurol. Sci.*, 1995, **129**, 107; R. B. Parsons, R. H. Waring, D. B. Ramsden and A. C. Williams, *Neurotoxicology*, 1998, **19**, 599.
- [4] J. G. McCoy, L. J. Bailey, E. Bitto, C. A. Bingman, D. J. Aceti, B. G. Fox and G. N. Phillips Jr., *Proc. Natl. Acad. Sci.*, 2006, **103**, 3084; J. A. Crawford, W. Li and B. S. Pierce, *Biochemistry*, 2011, **50**, 10241; S. C. Chai, J. R. Bruyere and M. J. Maroney, *J. Biol. Chem.*, 2006, **281**, 15774.
- [5] M. Costas, M. P. Mehn, M. P. Jensen and L. Que, Jr., *Chem. Rev.*, 2004, **104**, 939; D. Buongiorno and G. D. Straganz, *Coord. Chem. Rev.*, 2013, **257**, 541; S. Sahu and D. P. Goldberg, *J. Am. Chem. Soc.*, 2016, **138**, 11410.
- [6] P. C. A. Bruijninx, G. van Koten and R. J. M. Klein Gebbink, *Chem. Soc. Rev.*, 2008, **37**, 2716; S. Paria, L. Que, Jr. and T. K. Paine, *Angew. Chem. Int. Ed.*, 2011, **50**, 11129.
- [7] Y. M. Badiei, M. A. Siegler and D. P. Goldberg, *J. Am. Chem. Soc.*, 2011, **133**, 1274.
- [8] Y. B. Jiang, L. R. Widger, G. D. Kasper, M. A. Siegler and D. P. Goldberg, *J. Am. Chem. Soc.*, 2010, **132**, 12214; A. C. McQuilken, Y. Jiang, M. A. Siegler and D. P. Goldberg, *J. Am. Chem. Soc.*, 2012, **134**, 8758; A. C. McQuilken, Y. Ha, K. D. Sutherland, M. A. Siegler, K. O. Hodgson, B. Hedman, E. I. Solomon, G. N. L. Jameson and D. P. Goldberg, *J. Am. Chem. Soc.*, 2013, **135**, 14024; L. R. Widger, Y. Jiang, M. A. Siegler, D. Kumar, R. Latifi, S. P. de Visser, G. N. L. Jameson and D. P. Goldberg, *Inorg. Chem.*, 2013, **52**, 10467.
- [9] M. Sallmann, I. Siewert, L. Fohlmeister, C. Limberg and C. Knispel, *Angew. Chem. Int. Ed.*, 2012, **51**, 2234; M. Sallmann, B. Braun and C. Limberg, *Chem. Commun.*, 2015, **51**, 6785.
- [10] A. Fischer, N. Stracey, S. V. Lindeman, T. C. Brunold and A. T. Fiedler, *Inorg. Chem.*, 2016, **55**, 11839.
- [11] Santoro, C. Sarnbiagio, P. C. McGowan, and M. C. Halcrow, *Dalton Trans.*, 2015, **44**, 1060; A. Maleckis, L. F. Szczepura, L. M. Witham, K. J. Takeuchi, *Coord. Chem. Rev.*, 1998, **174**, 5. D. L. White and J. W. Faller *Inorg. Chem.* 1982, **21**, 3119.
- [12] M. K. Kashif, M. Nippe, N. W. Duffy, C. M. Forsyth, C. J. Chang, J. R. Long, L. Spiccia, and U. Bach, *Angew. Chem. Int. Ed.*, 2013, **52**, 1; J. Perez, D. Morales, L. A. Garcia-Escudero, H. M. Garcia, D. Miguel and P. Bernad, *Dalton Trans.*, 2009, **0**, 375; J. C. Knight, S. Alvarez, A. J. Amoroso, P. G. Edwards and N. Singh, *Dalton Trans.*, 2010, **39**, 3870; H. M. Berends, A. M. Manke, C. Näther, F. Tuzcek and Philipp Kurz, *Dalton Trans.*, 2012, **41**, 6215; F. R. Keene, J. M. R. Snow, P. J. Stephenson and E. R. T. Tiekink, *Inorg. Chem.* 1988, **27**, 2040; T. Astley, M. A. Hitchman, F. R. Keene and E. R. T. Tiekink, *J. Chem. Soc., Dalton Trans.*, 1996, 1845.
- [13] Gerald Dyker and Oliver Muth, *Eur. J. Org. Chem.* 2004, 4319; J. P. Bigi, T. E. Hanna, W. H. Harman, A. Chang and C. J. Chang, *Chem. Commun.*, 2010, **46**, 958; D. Wiedemann and A. Grohmann, *Dalton Trans.*, 2014, **43**, 2406; X. Li, C. L. D. Gibb, M. E. Kuebel and Bruce C. Gibb, *Tetrahedron*, 2001, **57**, 1175; D. Wiedemann and A. Grohmann, *Z. Anorg. Allg. Chem.* 2014, **640**, 1632; D. Wiedemann, E. Swietek, W. Macyk, and A. Grohmann, *Z. Anorg. Allg. Chem.* 2013, **639**, 1483–1490.
- [14] W. Li, E. J. Blaesi, M. D. Pecore, J. K. Crowell and B. S. Pierce, *Biochemistry*, 2013, **52**, 9104.
- [15] H. Stratemeier, M. A. Hitchman, P. Comba, P. V. Bernhardt and M. J. Riley, *Inorg. Chem.*, 1991, **30**, 4088; P. Comba, Y.-M. Lee, W. Nam and A. Waleska, *Chem. Commun.*, 2014, **50**, 412; J. Bautz, P. Comba and L. Que Jr., *Inorg. Chem.*, 2006, **45**, 7077; J. A. Kovacs, *Chem. Rev.* 2004, **104**, 825.
- [16] Y. Liu, T. Harlang, S. E. Canton, P. Chabera, K. S.-. Alcantara, A. Fleckhaus, D. A. Vinthang, E. Göransson, A. Corani, R. Lomoth, V. Sundström and K. Wärnmark, *Chem. Commun.* 2013, **49**, 6412.
- [17] E. J. Blaesi, B. G. Fox and T. C. Brunold, *Biochemistry*, 2014, **53**, 5759.
- [18] M. R. Bukowski, P. Comba, C. Limberg, M. Merz, L. Que Jr. and T. Wistuba, *Angew. Chem. Int. Ed.*, 2004, **43**, 1283.
- [19] M. D. Clay, F. E. Jenney, Jr., P. L. Hagedoorn, G. N. George, M. W. Adams and M. K. Johnson, *J. Am. Chem. Soc.*, 2002, **124**, 788.
- [20] G. V.-. Acevedo, E. Nam, S. Fitch, J. Benedict, J. Freudenthal, W. Kaminsky and J. A. Kovacs, *J. Am. Chem. Soc.*, 2011, **133**, 1419.
- [21] S. Hong, Y.-M. Lee, K.-B. Cho, M. S. Seo, D. Song, J. Yoon, R. G.-. Serres, M. Clemancey, T. Ogura, W. Shin, J.-M. Latour and W. Nam, *Chem. Sci.*, 2014, **5**, 156.
- [22] S. Pierce, J. D. Gardner, L. J. Bailey, T. C. Brunold and B. G. Fox, *Biochemistry*, 2007, **46**, 8569; C. R. Simmons, K. Krishnamoorthy, S. L. Granett, D. J. Schuller, J. E. Dominy, Jr., T. P. Begley, M. H. Stipanuk and P. A. Karplus, *Biochemistry*, 2008, **47**, 11390; C. M. Driggers, R. B. Cooley, B. Sankaran, L. L. Hirschberger, M. H. Stipanuk and P. A. Karplus, *J. Mol. Biol.*, 2013, **425**, 3121.
- [23] J. Cramer, W. B. Tolman, K. H. Theopold, and A. L. Rheingold, *Proc. Natl. Acad. Sci. USA.*, 2003, **100**, 3635; M. K. Coggins and J. A. Kovacs *J. Am. Chem. Soc.*, 2011, **133**, 12470; T. Kitagawa, A. Dey, P. Lugo-Mas, J. B. Benedict, W. Kaminsky, E. Solomon and Julie A. Kovacs *J. Am. Chem. Soc.*, 2006, **128**, 14448; Andris R. Navratil, J. Jasik, M. Puri, M. Costas, L. J. Que and J. Roithova *J. Am. Chem. Soc.*, 2018, **140**, 14391; X. Wang and L. Andrews *J. Phys. Chem. A*, 2006, **110**, 10035-10045; W. Nam, *Acc. Chem. Res.* 2015, **48**, 2415-2423; N. Lehnert, R. Y. N. Ho, L. Que Jr., E. I. Solomon, *J. Am. Chem. Soc.* 2001, **123**, 12802-12816; J. Cho, S. Jeon, S. A. Wilson, L. V. Liu, E. A. Kang, J. J. Braymer, M. H. Lim, B. Hedman, K. O. Hodgson, J. S. Valentine, E. I. Solomon, W. Nam, *Nature*, 2011, **478**, 502-505.
- [24] B. S. Furniss, A. J. Hannaford, P. W. Smith and A. R. Tatchwell, *Vogel's Textbook of practical Organic Chemistry*, 5<sup>th</sup> Edition. PEARSON Education Limited, New Delhi, **2004**, p 40.
- [25] E. A. Ünal, D. Wiedemann, J. Seiffert, J. P. Boyd and A. Grohmann, *Tetrahedron Letters*, **2012**, **53**, 54; b) A. Maleckis, J. W. Kampf and M. S. Sanford, *J. Am. Chem. Soc.*, **2013**, **135**, 6618.
- [26] R. T. Jonas and T. D. P. Stack, *Inorg. Chem.*, **1998**, **37**, 6615; J. P. Wibaut, A. P. De Jonge, H. G. P. Van der Voort, P. H. L. Otto, *Recl. Trav. Chim. Pays-Bas* 1951, **70**, 1054.
- [27] (a) K. Kabsch, in: M. G. Rossmann, E. Arnold (eds.), "International Tables for Crystallography" Vol. F, Ch. 11.3, Kluwer Academic Publishers, Dordrecht, **2001**. (b) *CrysAlisPro*, Agilent Technologies UK Ltd., Oxford, UK **2011-2014** and Rigaku Oxford Diffraction, Rigaku Polska Sp. z o.o., Wrocław, Poland **2015-2016**.
- [28] (a) R. H. Blessing, *Acta Cryst.* **1995**, **A51**, 33. (b) *SCALE3 ABSPACK*, *CrysAlisPro*, Agilent Technologies UK Ltd., Oxford, UK **2011-2014** and Rigaku Oxford Diffraction, Rigaku Polska Sp. z o.o., Wrocław, Poland **2015-2016**. (c) W. R. Busing, H. A. Levy, *Acta Cryst.* **1957**, **10**, 180.
- [29] (a) L. Palatinus, *SUPERFLIP*, EPF Lausanne, Switzerland and Fyzikální ústav AV ČR, v. v. i., Prague, Czech Republic, **2007-2014**; (b) L. Palatinus, G. Chapuis, *J. Appl. Cryst.* **2007**, **40**, 786.
- [30] (a) G. M. Sheldrick, *SHELXL-20xx*, University of Göttingen and Bruker AXS GmbH, Karlsruhe, Germany **2012-2016**; (b) G. M. Sheldrick, *Acta Cryst.* **2008**, **A64**, 112; (c) G. M. Sheldrick, *Acta Cryst.* **2015**, **C71**, 3.
- [31] D. F. Evans, *J. Chem. Soc.*, **1959**, 2003.
- [32] R. Mayilmurugan, H. S. Evans and M. Palaniandavar, *Inorg. Chem.*, **2008**, **47**, 6645.
- [33] a) Japan Chemical Society, *Kagaku-Binran Basic Part II*, 2nd ed, Maruzen: Tokyo, **1975**; b) D. T. Sawyer, *Oxygen Chemistry*, Oxford University Press: New York, **1991**.
- [34] W. O. Koch and H. J. Krüger, *Angew. Chem., Int. Ed. Engl.*, **1995**, **34**, 2671.

## FULL PAPER

- [35] M. J. Frisch, *et al*, Gaussian 09, revision D. 01. Gaussian, Inc., Wallingford, CT, **2009**.
- [36] A. D. Becke, *J. Chem. Phys.* **1993**, *98*, 5648–5652.
- [37] C. Lee, W. Yang, R. G. Parr, *Phys. Rev. B* **1988**, *37*, 785–789.
- [38] M. Jaccob, G. Rajaraman, *Dalton Trans.* **2012**, *41*, 10430-10439.
- [39] B. Pandey, M. Jaccob, G. Rajaraman, *Chem. Comm.* **2017**, *53*, 3193-3196.
- [40] M. A. Marques,.; E. K. Gross, *Annu. Rev. Phys. Chem.* **2004**, *55*, 427-455
- [41] J. Tomasi, B. Mennucci, R. Cammi, *Chem. Rev.* **2005**, *105*, 2999-3094.
- [42] S. Miertuš, E. Scrocco, J. Tomasi, *Chem. Phys.* **1981**, *55*, 117-129.

WILEY-VCH

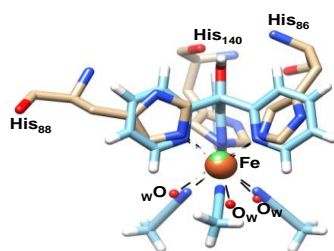
Accepted Manuscript

## FULL PAPER

## Entry for the Table of Contents

## FULL PAPER

The iron(II) complexes of a tris(2-pyridyl)-based ligand are presented as accurate structural models for cysteine dioxygenase (CDO). With O<sub>2</sub> they selectively convert sulfur-based substrates into doubly oxygenated products via a Fe<sup>III</sup>-peroxido reaction intermediate.



Karunanithi Anandababu,  
Ramamoorthy Ramasubramanian,  
Hubert Wadepohl, Peter Comba\*,  
Neethinathan Johnee Britto,  
Madhavan Jaccob and Ramasamy  
Mayilmurugan\*

*Page No. – Page No.*

**A Structural and Functional Model  
for the Tris-Histidine Motif in  
Cysteine Dioxygenase**